Spectrochimica Acta Part B 148 (2018) 129–136

Contents lists available at ScienceDirect

Spectrochimica Acta Part B

journal homepage: www.elsevier.com/locate/sab

Review article

Recent advances in surface elemental mapping via glow discharge atomic spectrometry

Gerardo Gamez*, Kevin Finch

Texas Tech University, Department of Chemistry and Biochemistry, Lubbock, TX 79409-41061, USA

ABSTRACT

Glow discharge atomic spectrometry has been very popular for direct solid, quantitative, conductive and non-conductive materials characterization. Lateral resolution capabilities, however, have been very limited. Described in this review are the advantages and current limitations of glow discharge surface elemental mapping, coupled with optical emission or mass spectrometry, along with recent advances in measurement strategies to overcome many of the conventional limitations. Recent applications, including glow discharge optical emission spectroscopy (GDOES) ultra-high throughput elemental mapping of thin films and combinatorial libraries utilizing glow discharge as an excitation source are presented. Also, current advances for extending the lateral and depth resolution capabilities of GDOES elemental mapping to larger samples by adapting the discharge chamber design are discussed. In addition, the realization of glow discharge mass spectrometry (GDMS) elemental mapping through a pixel-by-pixel rastering method is reviewed, along with the potential advantages. Furthermore, the three-dimensional elemental mapping capabilities recently displayed by GDOES are considered to show the future trends, which include the potential of allowing elemental mapping protocols previously reserved for fundamental studies to be implemented for routine diagnostic mapping of high sample numbers.

1. Introduction

Glow discharge spectrometry (GDS) has created a niche in elemental analysis because of its many advantages, including direct solid, simultaneous multi-elemental, qualitative and quantitative analysis over a wide dynamic range [1, 2]. In addition, it enjoys several favorable practical aspects such as high-throughput analysis, due to the fast sputtering rates and multi-matrix calibration, applicability to a variety of sample types, and low running costs [3, 4]. Furthermore, it is not just a bulk analysis technique, but its depth-profiling capabilities have been maturing to achieve resolution in the nanometer scale [5]. Also, it allows analysis of light elements like H, O, C, and N, where most other techniques fail.

Nevertheless, one area where GDS has been limited is with regards to laterally resolved analysis for elemental mapping [6]. Elemental mapping is key to improve our understanding of the consequences and origins of chemical heterogeneity on the function, as well as mechanisms, of natural and manufactured systems [7]. As such, there have been many recent advances in elemental analysis techniques in pursuit of better performance with respect to mapping capabilities [8–13]. In traditional GDS, the material sputtered from the same layer in the sample is blended in the discharge, while the sampling crater is limited in commercial GDS systems to diameters in the mm scale. Thus, obtaining laterally resolved information with traditional GDS would require a method to raster pixel-by-pixel, while breaking vacuum conditions between measurements, which would require an impractical amount of time, while yielding lateral resolution in the mm scale. However, mixing in the discharge of sputtered atoms from the same layer in the sample is not complete. Optical emission intensity heterogeneities from heterogeneous samples have been identified in traditional GDS [14] and some efforts have been proposed to minimize the effect [15].

Operating the GD under pulsed-power conditions has been shown to afford several advantages [16]. For example, it is possible to apply higher instantaneous power without inflicting major thermal damage to the sample, which may improve analytical performance while allowing analysis of thermally labile samples. In addition, pulsed-power conditions reduce the sputtering rates which may be beneficial for depth resolution. Moreover, temporally resolved detection permits obtaining the analytical signal at different times along the power pulse which may result in better signal-to-noise ratios for selected analytes. Pulsed-power conditions have also been observed to enhance the optical emission heterogeneities from heterogeneous samples and together with higher operating pressures, also shown to further enhance the effect, yield

* Corresponding author.
E-mail address: gerardo.gamez@ttu.edu (G. Gamez).

https://doi.org/10.1016/j.sab.2018.06.015
Received 30 May 2018; Received in revised form 19 June 2018; Accepted 21 June 2018
Available online 22 June 2018
0584-8547/

laterally resolved sample information from within the GD sputtered crater [6]. The lateral resolution capability has allowed GDOES elemental mapping to be developed which, on top of sharing the advantages of traditional GDS, offers the possibility of ultra-high throughput imaging, orders of magnitude faster vs other techniques [17].

In this review, we aim to cover the progress that has taken place in the area of GDS elemental mapping since the last time the topic was reviewed, more than five years ago [6]. Herein, advances in instrument development, novel applications, as well as unique strategies made possible by the newly available lateral resolution in GDS will be discussed.

2. Instrumentation advances

One of the most significant advantages of GDOES elemental mapping is the ultra-high throughput imaging capabilities. One disadvantage that traditional elemental mapping techniques relying on pixel-by-pixel rastering, such as secondary-ion mass spectrometry (SIMS) or laser ablation inductively coupled plasma mass spectrometry (LA-ICP-MS), share is the long acquisition time needed to obtain a full elemental map, which gets worse as the pixel density and size of the sampled area increases. A study from 2007 using time-of-flight (ToF) SIMS as a high-throughput elemental mapping technique shows an analysis time of 1.5 h for an area of 128 × 128 pixels [18]. A more recent study from 2016 using LA-ICP-ToFMS obtained a 2D elemental map of Fe, Ca, and Al in 7.5 min for 5000 total pixels [11]. Consequently, elemental mapping has been limited to mechanistic/fundamental studies of a few samples while routine diagnostic-based imaging, when there are many samples, has remained elusive. The throughput limitations, besides those unique to each technique, arise from having to collect the elemental information by rastering sequentially from pixel-to-pixel to obtain the three-dimensional hyperspectral data cube. GDOES elemental mapping allows the collection of two dimensions simultaneously, and only requires one dimension to be scanned. Thus, a 350 × 512 pixel elemental map can be obtained by GDOES in as few as 42 s (see below), while with the sampling rates reported using the techniques mentioned above, it would take over 16 h with SIMS and 4.5 h with LA-ICPMS. It is evident that the higher-throughput advantage of GDOES elemental mapping becomes even more significant as the size of the sampled area and the pixel density increase. On the other hand, commercial GDOES systems only offer sampled areas from 1 mm to 8 mm in diameter [3]. Therefore, several efforts have been taking place to make possible the elemental mapping of large diameter samples via GDOES.

Voronov and co-workers studied the effects of sustaining a large-diameter glow discharge under conditions favorable for OES elemental mapping, including pulsed-power and higher pressures (0.5–20 hPa) [19]. They showed that for an 80 mm diameter sample a stable discharge can be achieved under continuous rf power operation and at 100 Pa (Fig. 1a). On the other hand, unstable discharge heterogeneities appear when the pressure is increased to 400 Pa (Fig. 1b). An increase in the length of their anode extension and operating under pulsed-power conditions caused the heterogeneities to become smaller and localize at the edge of the cathode area (Fig. 1c). The authors use cathode boundary layer micro-discharges literature to point to self-organization theory as a possible way to explain the heterogeneities found in their results and alternatively point to discharge contraction, although the authors note the operating modes are not similar. They arrive at a more stable discharge with a 40 mm diameter sample at 18 hPa.

Kroschk et al. also explored the possibility of increasing the size of the discharge to allow larger diameter samples to be mapped via GDOES [20]. They observed a stable and homogenous discharge for a 100 mm diameter sample at 267 Pa under pulsed rf power. As expected, discharge heterogeneities appeared when the pressure was increased, as their data shows at 1870 Pa. The authors note that increasing distances between the cathode axis and the anode, together with the plasma contraction at higher pressures, are giving rise to the discharge heterogeneities. As such, they propose a restrictive anode array mask (RAAM) GD geometry to permit mapping of large diameter samples. In short, the RAAM is a grounded thick conductive plate with an array of apertures placed about a hundred microns from the sample. Thus, the RAAM functions as an anode allowing an array of glow discharges to be formed within the apertures but restricting discharge formation everywhere else (Fig. 2A, B). As such, the distance from the anode to the cathode axis is shortened, which prevents the above-mentioned discharge unstable heterogeneities from arising when the operating the GD at higher pressures. It should be noted that, as opposed to the glow discharge array design by Winchester and Salit [21], the lateral resolution in RAAMs does not originate from the size of each aperture but from the pulsed-power/higher pressure operation, which allows mapping within each aperture. The authors optimize the aperture i.d., plate thickness, inter-aperture spacing, and grounding configuration to allow GDOES elemental mapping of a 100 mm diameter model sample at 2130 Pa (Fig. 2C).

There have also been some efforts into improving the spectral imaging system used to collect laterally resolved optical emission from the GD. Previously, three different imaging systems have been implemented and their merits with respect to GDOES elemental mapping have been discussed [6]. First, a monochromatic imaging spectrometer [22–24] (MIS), staring-type imager, was implemented where the collected light is collimated then passed through a monochromator and refocused onto an array detector, such that the monochromator serves as a wavelength-tunable bandpass filter. The MIS advantage is wavelength selection flexibility, on the other hand, it delivers low light throughput at increasing spectral resolution, due to the effect of the slit, and slow sequential wavelength scan-speed with typical monochromators. Second, an acousto-optic tunable filter (AOTF), staring-type, spectral imager was demonstrated. The AOTF is in essence a variable grating acoustically controlled on a birefringent crystal which has the advantage of random-wavelength access within microseconds and a much higher light throughput vs the typical MIS, but crystal performance is very limited in the VUV region, its bandpass varies with

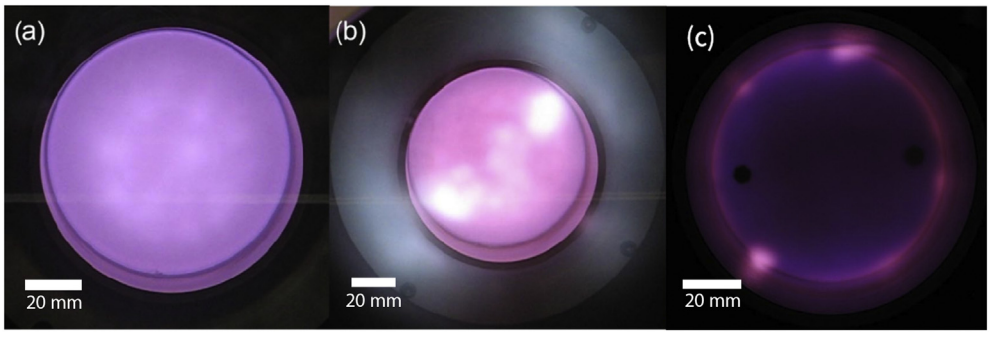

Fig. 1. Front view of an 80 mm GD sample showing unstable heterogenieties, continuous 13.56 MHz rf discharge, 70 W applied power, at (a) 100 Pa pressure and (b) 400 Pa pressure. (c) 80 mm GD sample with an increased anode extension, pulsed 13.56 MHz rf discharge, 100 Hz pulse frequency, 100 μs transient time, 100 Pa Pressure, and 500 V peak-to-peak. [19] - Adapted by permission of The Institute of Physics.

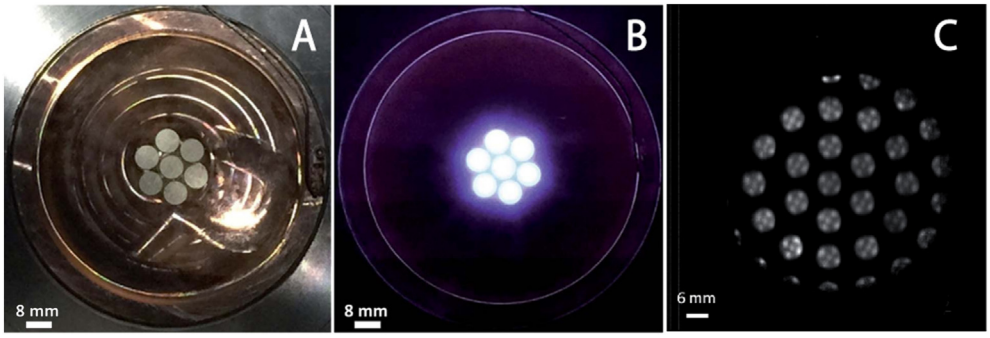

Fig. 2. Seven aperture RAAM positioned a few hundred microns from sample with GD power off (A) and during GD operation showing minimized heterogeneities under optimized elemental mapping conditions (B). (C) RAAM GDOES Ag elemental emission map at 328.1 nm using a 6 mm i.d. aperture, at a 2130 Pa pressure, 4 W mm^{-2} power density, 16 µs pulse duration, and an ICCD camera with 10 µs gate width, 6 µs delay. [20] - Adapted by permission of The Royal Society of Chemistry.

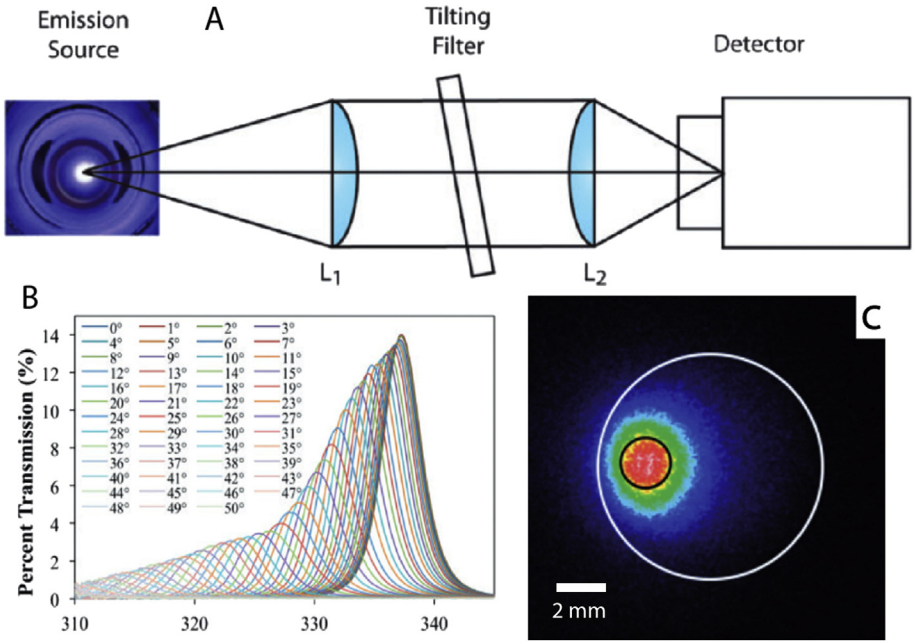

Fig. 3. (A) High optical throughput tilting interference filter utilized as a wavelength selection device to characterize GDOES elemental emission maps with spatially resolved information. (B) Transmission characteristics for a span of wavelengths between 310 nm and 345 nm at different tilt angles from the normal of the interference filter. (C) Optical emission image at 328.1 nm showing the laterally resolved position for the Al sample with a pure Ag pin, with no spectral interferences. [27] - Adapted by permission of SAGE.

wavelength and it relies heavily on polarizer efficiency [25]. Third, a push-broom hyperspectral imager (PBHSI) was employed, where the collected image is directed to the entrance slit of a spectrograph and only a "column" section of the image goes through such that the information in the y-dimension and the λ-dimension are obtained simultaneously, while the x-dimension is obtained sequentially by scanning the image over the entrance slit. The advantages of the PBHSI include high optical throughput capabilities, but it is limited in the spectral window covered simultaneously for each hyperspectral data cube [26]. Recently, Storey et al. implemented a tilting interference filter as a wavelength selection device in place of the monochromator in an MIS configuration for GDOES elemental imaging [27]. The advantage of such a system lies in its high optical throughput with very little complexity (Fig. 3A). The interference filter used for proof-of-principle had a design central wavelength at 337.59 nm and it could be tuned down, by changing the light incidence angle, more than 22 nm with a corresponding lower percent transmission as shown in Fig. 3B. The authors show optical emission maps at 338.3 nm and 327.4 nm of a Ag pin embedded in an Al (Fig. 3C) or brass substrate. Although the filter bandpass is about 3 nm, several specific applications could greatly benefit from the high optical throughput, low complexity and cost efficiency.

Kroschk et al. implemented an improved PBHSI system [20]. The PBHSI used previously by Gamez et al. [26] suffered from significant smile (curvature of the slit image) with a peak shift of 33.28 µm in the middle, 46.08 µm at the upper limit and 53.76 µm at the lower limit of the field of view. Field curvature was also a factor which required the authors to increase the f/# (from 3.88 to 16) of the spectrograph to sufficiently minimize the effects and achieve appropriate spectral resolution (0.4 nm–0.8 nm) throughout the field of view, but at a cost of light throughput. The newer system by Kroschk et al. uses a Czerny-Turner-Schmidt spectrograph where the aberrations are minimized and the spectral resolution is better in a much bigger field-of-view while keeping the f/# at 4.6 (Fig. 4).

Other efforts to achieve elemental mapping capabilities with glow discharges have taken place with mass spectrometry detection. Konarski et al. used an xyz high-vacuum translation stage within a membrane bellow to allow in situ movement of the sample with respect to a GD lamp coupled to a quadrupole mass analyzer (Fig. 5A) [28]. The elemental maps are obtained in a pixel-by-pixel fashion, but the translation stage allows this to be achieved continuously without having to break vacuum when moving to the next pixel, which improves greatly on sample throughput. The authors discuss the potential consequences of the rastering approach on the sputtered crater shape, including the effects of a having a concave crater shape and the subsequent roughness induced as a function of raster scan line density. They go on to show GDMS multi-elemental maps of two model samples with heterogeneity in one dimension (stripe structures) or two dimensions (concentric circular structures), as shown in the insets of Fig. 5B, C. One thing to note is that the lateral resolution in their system (0.16 mm–0.42 mm along the raster dimension) is restricted in part by a mask between the GD anode and sample cathode, as well as the raster step size. Furthermore, the scanning nature of quadrupole mass analyzers presents some limitations when it comes to multi-elemental

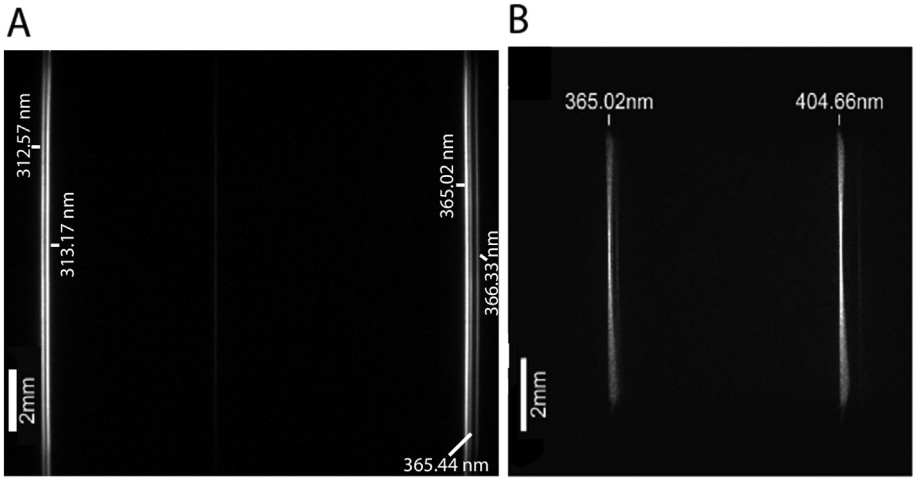

Fig. 4. (A) Mercury pen lamp emission spectrum imaged using a PBHSI featuring a Czerny-Turner-Schmidt spectrograph, compared to a previous spectral image (B) obtained with a typical Czerny-Turner spectrograph with comparable f/#. Differences in aberration minimization are evident.

analysis. Nevertheless, the GDMS elemental mapping technique could be implemented on other mass analyzers to improve the overall performance. Albeit pixel-by-pixel rastering is inherently time consuming, GDMS offers several advantages over GDOES, including isotopic analysis and the possibility of obtaining molecular information [5, 29–31]. Moreover, GDMS allows the analysis of some elements (e.g. oxygen, nitrogen, etc.) which may have limitations with other traditional elemental mapping techniques.

3. Applications

Recent application developments in GDOES elemental mapping have taken place in the area of materials characterization, more specifically in thin films [17, 32]. Thin films are used in a variety of fields [33–36], including optics, semi-conductors, energy conversion, and energy storage, just to mention a few. The spatial composition heterogeneity is critical for the thin film performance, for example, from the stoichiometry of major elements to the distribution of dopants. Furthermore, thin films have become the platform for the study of materials combinatorial libraries, where thin film spatial composition gradients allow for the accelerated discovery of new materials and their properties [37]. The sheer volume and spatial complexity of high-throughput combinatorial techniques require a temporally efficient, spatially resolved system for analysis, for which GDOES elemental mapping has proven to be a good candidate.

Gamez et al. investigated the use of a restrictive anode end-on Grimm type geometry GD, operating in direct current (dc) pulsed-power mode, coupled to a push-broom hyperspectral imaging system (PBHSI) for ultra-high throughput thin film combinatorial library elemental mapping [17]. They showed that a hyper-spectral data cube of the GDOES image map from a CuNi composition spread (x = 350 pixels, y = 512 pixels, 305 nm to 375 nm spectral window) was obtained in just 42 s (Fig. 6A). The analysis time is several orders of magnitude faster compared to traditional elemental mapping techniques, taking into account the pixel density [17]. Furthermore, quantitative analysis was achieved through the emission yield concept [38, 39], which was applied for the first time for elemental mapping purposes, by fitting an independent calibration curve to each pixel through calibration coefficient matrix-images (Fig. 6B, C). The advantage of this type of pixel-by-pixel calibration is that it takes into account any variations which would otherwise have to be calibrated independently, for example, variations in the flatness of the field-of-view or detector pixel gain, and even the natural variations in emission intensity originating in the GD.

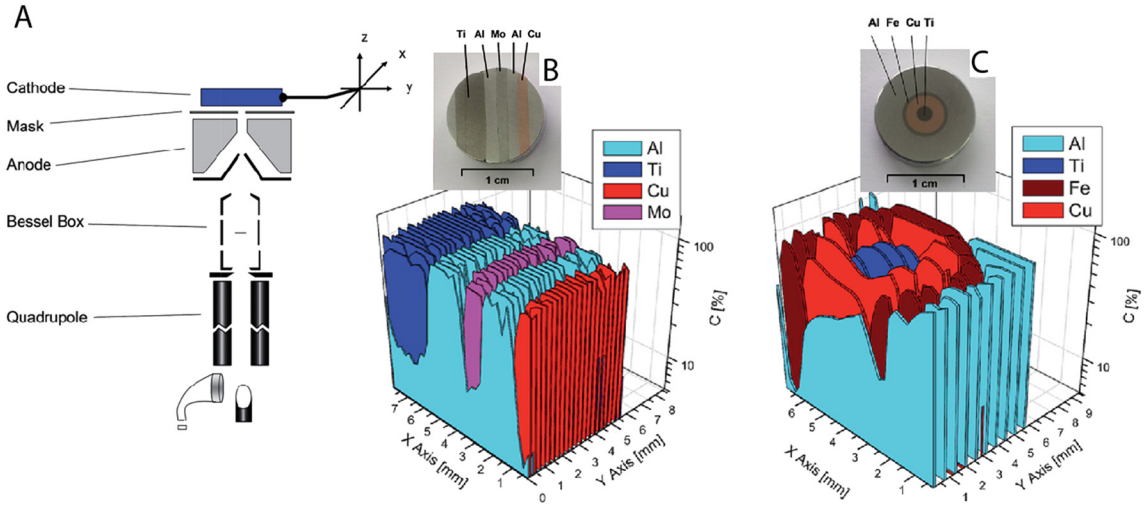

Fig. 5. (A) 2D imaging GDMS consisting of a GD lamp coupled to a quadrapole mass analyzer by a translation stage within a membrane bellow for in situ movement. Raster scans of the model samples containing Ti, Cu, and Mo stripes (B) and Fe, Cu, and Ti concentric structure (C) embedded in an Al substrate. [28] - Adapted by permission of The Royal Society of Chemistry.

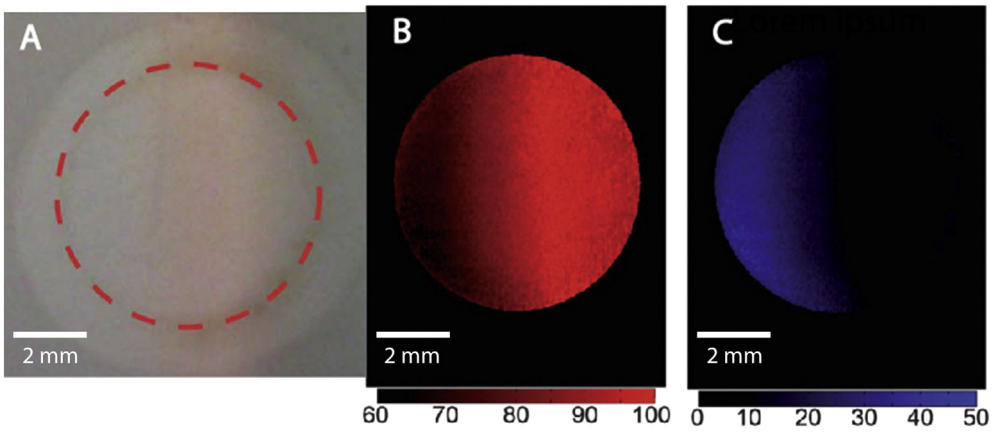

Fig. 6. (A) CuNi thin film composition spread showing the analyzed region of interest within the red dotted circle. (B) Quantitative GDOES elemental map (wt%) for Cu and (C) Ni obtained within the region of interest (ROI). [17] - Adapted by permission of The Royal Society of Chemistry. (For interpretation of the references to color in this figure legend, the reader is referred to the web version of this article.)

The quantitative GDOES elemental maps showed the Cu concentration increasing from about 60% to close to 100% from left to right, while the Ni concentration varies from about 40% to 0% in the same direction. The authors verified their quantitative results from GDOES by performing energy-dispersive X-ray spectroscopy (EDX) to obtain an elemental composition single-line profile, which shows very similar concentration gradients. This study showed GDOES elemental mapping to be several orders of magnitude faster than typical techniques and its effectiveness for thin film and materials combinatorial library imaging.

Gonzales et al. expanded ultrafast elemental mapping of GDOES to nitrogen-based combinatorial libraries with non-conductive samples, through the implementation of pulsed-power mode radiofrequency (rf) and the coupling of a PBHSI to a restrictive anode end-on Grimm type geometry GD, for spatially resolved analysis of a AlN-CrN thin film composition gradient [32]. In this case, a spectral window of 376 nm to 446 nm allowed measuring Al and Cr lines simultaneously while an applied plasma power of 80 W allowed improved emission intensities and sputtering rates for the AlN-CrN thin film, while being able to obtain (x = 323 pixels, y = 512 pixels) elemental composition maps in just 16.8 s. Semi-quantitative elemental maps for Al and Cr were also obtained through the constant emission yield concept as in [17] (Fig. 7A, B). It is important to note, however, that the N content was not determined directly because the vacuum UV range was inaccessible by the imaging system, thus N content was indirectly calculated by normalizing all species to a total of 100%. Nevertheless, a commercial GDOES instrument was utilized for comparative analysis and showed good agreements for the concentration results of Al, N, and Cr.

Matsuura et al. explored the possibility of using spatially resolved end-on GDOES detection to obtain laterally resolved information from a square 1 mm × 1 mm Cu sample placed on a Ni substrate, inside a 8 mm anode Grimm type discharge chamber [40]. They operated GD under pulsed dc conditions with a peak voltage of 400 V, 1 ms pulse duration with varying duty cycle, and an Ar pressure of 530 Pa. The lateral resolution obtained, however, was very low, mainly due to the operating conditions with pulse duration orders of magnitude longer, and pressures several times lower, compared to optimized GDOES elemental mapping conditions [6].

4. Three-dimensional surface elemental mapping

The lateral elemental mapping capabilities of GDS give rise to unique and novel strategies, for example, three-dimensional elemental mapping. The sputtering nature of glow discharge spectroscopy

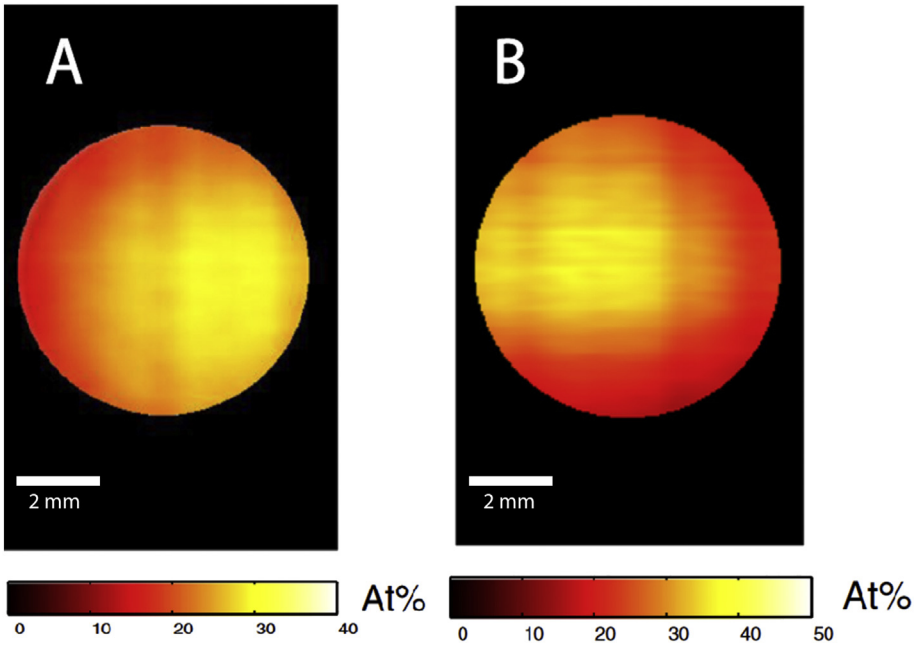

Fig. 7. (A) Quantitative GDOES elemental map (at.%) for Al and (B) Cr obtained for the AlN-CrN thin film composition spread over the area of interest. [32] - Adapted by permission of Springer.

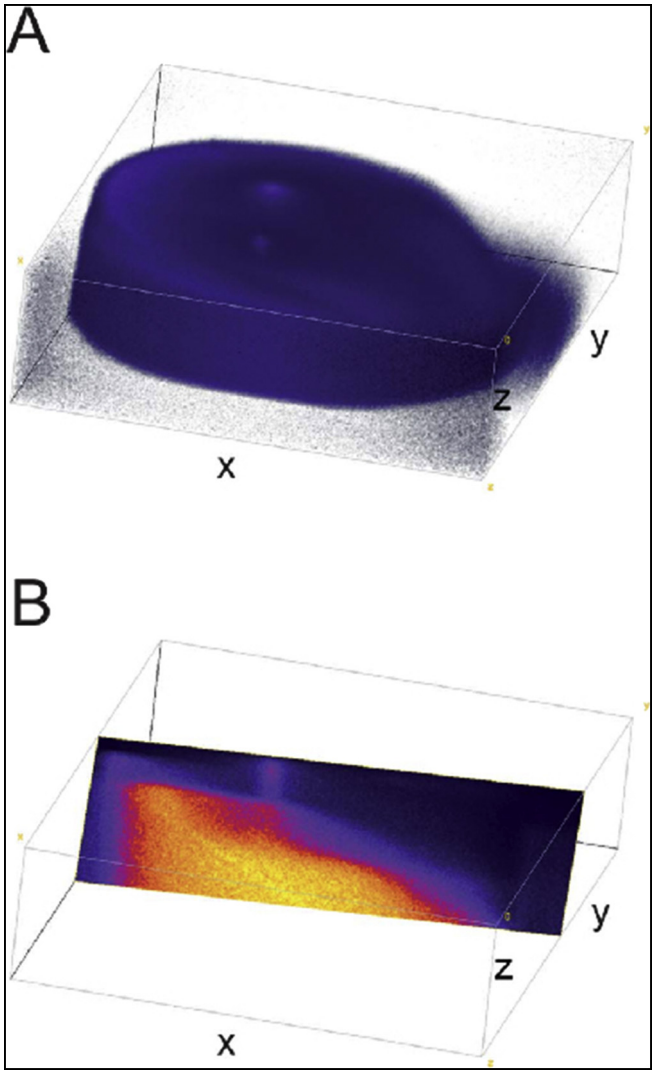

Fig. 8. (A) Qualitative GDOES emission map at 341.5 nm in 3D from a perforated Cu thin film deposited on a Ni substrate. (B) 2D slice showing Ni emission across the 3D GDOES emission map in (A). [41] - Reproduced by permission of The Royal Society of Chemistry.

removes layers of the sample surface and thus, when coupled to time resolved detection, it allows depth profiling to be performed. Gamez et al. showed the first example of three dimensional GDOES elemental mapping by collecting 100 consecutive two-dimensionally resolved elemental maps from the same sample [41]. Fig. 8A shows the qualitative 3D GDOES Ni emission map obtained from a Ni substrate sample with a perforated Cu thin film at the surface. The plane slice cross section (Fig. 8B) shows the Ni emission at 341.5 nm which appears in a small region at the surface and corresponds to the perforation in the Cu film. It is also evident that the Ni emission emerges faster on one side of the map, which is due to the Cu film thickness varying across the sampled area. In the case of GDOES, 3D elemental mapping analysis time becomes practical, even at high pixel densities, due to the ultra-high throughput of individual lateral maps which can be as fast as a few tens of seconds. Furthermore, the pulsed-power operation together with the high throughput of GDS elemental mapping allows for high depth resolution to be maintained, where one pixel in depth has been reported to be as small as 2.9 nm for a pure Cu sample, based on the average erosion rate of 12.5 nm min^{-1} by measuring the crater depth after 8 h of sputtering [26]. It should be noted that the depth resolution depends partially on surface roughness of the crater, which typically gets worse at greater depths. On the other hand, one of the most important aspects restricting depth resolution in commercial glow discharge systems is the sputtered crater shape [5, 42]. As discussed above, the sputtered material is combined in the discharge under typical operating conditions, thus if the crater bottom is not flat the materials from different layers are mixed in the plasma and the depth resolution is degraded. Nevertheless, it is possible to get very flat crater shapes by adjusting the GD electrical and pressure operating parameters. As such, it is commonplace to expect good depth resolution performance by GDS for thin and ultra-thin films, given the right conditions. Still, even when the GD operating conditions are adjusted to obtain a flat crater in certain material, and the material is assumed to be laterally homogeneous within the sputtered crater (1 mm–8 mm i.d.), crater shapes may change when going through multilayered samples [5]. 3D GDOES elemental mapping may offer a way to overcome such limitation because the laterally resolved information is maintained. Thus, one would be able to tell the layer from which the signal originated even if the crater shape is not ideally flat, within the restrictions of the lateral resolution. Characterizing the merits of such an approach is one of the areas currently being explored.

Nonetheless, it is important to keep the inherent limitations of GDS depth profiling in mind, such as surface roughness [1–5, 42]. Surface roughness may be a characteristic of the original sample or it may be induced through the sputtering process. Sputtering-induced surface roughening would be expected to arise from sample heterogeneity due to the difference in sputtering rates of different matrices. Quantification in GDOES depth-profiling, which works particularly well for alloys, is based on emission yield calibrations and calculation of sputter factors by normalizing to 100% [38, 39]. Conversion of sputtering time to sputtering depth relies on some assumptions regarding the material density and even some corrections may be applied for oxides, nitrides and carbides [43]. However, this approach cannot account for certain aspects, such as porosity. In fact, different crystal phases of the same material may have different sputtering rates. Thus, several efforts have been proposed to permit real-time depth measurements via interferometric profilometry during the sputtering process in order to correct for possible errors [43, 44]. It would be advantageous to apply a similar protocol to GDOES elemental mapping, even though interferometric depth measurements are limited to samples with high reflectivity.

5. Conclusions

It is evident that the development of elemental mapping capabilities via glow discharge spectroscopy has received a recent thrust due to the limitations of traditional techniques and the advantages GDS offers. In the case of GDOES, in addition to the inherent advantages, the unique ultra-high throughput elemental mapping capabilities stand out, which can be several orders of magnitude faster compared to traditional techniques, and become more significant in large samples. This presents the possibility of translating mapping protocols from performing fundamental and mechanistic studies, typically reserved for a few selected samples due to the throughput limitations of traditional techniques, toward developing routine diagnostic studies when required by numerous samples. In addition, the ultra-high throughput lateral mapping also presents the possibility of obtaining high pixel density 3D composition maps at high-speeds. On the other hand, GDMS mapping, also offers some unique advantages particularly with respect to isotopic analysis and molecular information, taking into account the inherent pixel-by-pixel long rastering-time limitations.

Then again, it is also apparent that further development is needed to be able to fully exploit the possible advantages of GDS elemental mapping. With respect to GDOES, instrument capabilities need to be developed to allow detection in the VUV region, which is critical for the analysis of C, H, N, S, and Cl. There are many applications that do not require such elements to be determined but having this capability opens the door for many other applications including oxide based semiconductors or hydrogen doped materials, etc.

Also, there is room for development of the GD lamp, for example, the RAAM geometry. One area currently being explored is allowing linear RAAM columns to be operated individually to permit sequential scanning which would result in lower power requirements and a higher duty cycle when coupled to PBHSI detection, thus improving depth resolution. In addition, original RAAMs were developed to overcome discharge instabilities with large area samples by decreasing anode-cathode distances but it does not necessarily have to be in 2 dimensions, i.e. circular apertures, thus slit-type apertures are currently being explored to increase the ratio of the measured vs. masked area.

Furthermore, implementation of alternate imaging systems may offer several advantages. For example, compressed sensing (CS) HSI approaches offer improved sampling throughput, or higher resolution in the dimension of interest [45]. In connection with sample throughput, CS relies on signal sparsity and group sampling of random combinations of pixels in the dimension of interest to allow compression during acquisition. Implementation of GDOES elemental mapping with a single pixel CS HSI [46] is currently being explored to improve accessibility while keeping a high sample throughput.

Additionally, having access to hyperspectral data cubes presents opportunities with respect to data analysis. For example, multi-variate calibration algorithms, which have been shown to yield superior calibration models vs univariate methods, even for complex spectra and in the presence of matrix interferences [47], can be implemented.

Moreover, application development needs to be advanced. For example, GDOES elemental mapping of biological thin sections would open the door for many applications. It has been shown previously that GDOES can be used for the bulk analysis of thin bone sections [48]. Thus, having 3D spatial resolution with ultra-high sample throughput would be quite significant. Regarding possible applications, it is worth considering the expected limits of detection. Typical LODs in GDOES range from 0.1–10 ppm. A threshold of expected LODs from GDOES elemental mapping can be estimated by assuming the background in GDOES is limited by the detector, which is not the case but will serve as a worst-case scenario. In this case, and using a PBHSI, the signal which was once collected by a single detector will now be across a column of ~100 pixels, thus giving higher LODs by possibly two orders of magnitude. However, the background is not detector limited because there is variable optical emission background which is wavelength and sample dependent [49]. Thus, it is more realistic to expect only an order of magnitude higher LODs which are competitive or better compared to XRF, EDS, PIXE, Auger, XPS, or even LIBS. Ultimately, LODs for GDOES elemental mapping need to be comprehensively determined. Nevertheless, it is also worth noting that obtaining spatially resolved information may lower the LOD burden for some applications. For example, the concentration of an inclusion in a steel sample would be diluted in the discharge under typical GDS conditions. On the other hand, GDOES elemental mapping operating conditions minimize such dilution such that higher LODs may prove sufficient for such analysis.

With respect to GDMS, implementing alternative mass analyzers would allow to overcome many of the limitations observed in the proof-of-principle study. For example, ToFMS has been shown to be very advantageous, due to the high-speed sampling rates, when applied to fast transient signals, such as those obtained when performing depth profiling by GDMS [5]. Implementing ToFMS to GD elemental mapping should afford analogous sample throughput gains. Also, operation in pulsed-power mode coupled to time-resolved detection allows for better analytical figures of merit for selected analytes. In addition, the pixel-by-pixel rastering nature of the GDMS mapping allows implementation of oversampling approaches, as in [13], to possibly improve the spatial resolution. Finally, there is a need for the development of applications that feature MS unique advantages, such as isotopic analysis and the possibility of obtaining direct molecular information.

Acknowledgements

The authors would like to acknowledge support by the National Science Foundation under CHE - 1610849.

References

[1] K.R. Marcus, J.A.C. Broekaert, Glow Discharge Plasmas in Analytical Spectroscopy, John Wiley & Sons, New York, 2003.
[2] R. Payling, D.G. Jones, A. Bengtson, Glow Discharge Optical Emission Spectrometry, John Wiley & Sons, Chichester, 1997.
[3] T. Nelis, R. Payling, Glow Discharge Optical Emission Spectroscopy : A Practical Guide, Royal Society of Chemistry, Cambridge, UK, 2003.
[4] A. Bengtson, Glow-discharge optical-emission spectroscopy, Surface Characterization: A User's Sourcebook, Wiley Blackwell, 2007, pp. 230–243.
[5] L. Lobo, B. Fernández, R. Pereiro, Depth profile analysis with glow discharge spectrometry, J. Anal. At. Spectrom. 32 (2017) 920–930.
[6] G. Gamez, M. Voronov, S. Ray, V. Hoffmann, G. Hieftje, J. Michler, Surface elemental mapping via glow discharge optical emission spectroscopy, Spectrochim. Acta B At. Spectrosc. 70 (2012) 1–9.
[7] F. Adams, C. Barbante, F. Adams, C. Barbante (Eds.), Chemical imaging introduction, Elsevier, 2015, pp. 1–27.
[8] M. Bonta, J.J. Gonzalez, C. Derrick Quarles, R.E. Russo, B. Hegedus, A. Limbeck, Elemental mapping of biological samples by the combined use of LIBS and LA-ICP-MS, J. Anal. At. Spectrom. 31 (2016) 252–258.
[9] B. Busser, S. Moncayo, J.L. Coll, L. Sancey, V. Motto-Ros, Elemental imaging using laser-induced breakdown spectroscopy: a new and promising approach for biological and medical applications, Coord. Chem. Rev. 358 (2018) 70–79.
[10] J.R. Chirinos, D.D. Oropeza, J.J. Gonzalez, H. Hou, M. Morey, V. Zorba, R.E. Russo, Simultaneous 3-dimensional elemental imaging with LIBS and LA-ICP-MS, J. Anal. At. Spectrom. 29 (2014) 1292–1298.
[11] A. Gundlach-Graham, D. Günther, Toward faster and higher resolution LA-ICPMS imaging: on the co-evolution of la cell design and ICPMS instrumentation (Young Investigators in Analytical and Bioanalytical Science), Anal. Bioanal. Chem. 408 (2016) 2687–2695.
[12] K. Tsuji, T. Matsuno, Y. Takimoto, M. Yamanashi, N. Kometani, Y.C. Sasaki, T. Hasegawa, S. Kato, T. Yamada, T. Shoji, N. Kawahara, New developments of X-ray fluorescence imaging techniques in laboratory, Spectrochim. Acta B At. Spectrosc. 113 (2015) 43–53.
[13] S.J.M. Van Malderen, J.T. van Elteren, F. Vanhaecke, Submicrometer imaging by laser ablation-inductively coupled plasma mass spectrometry via signal and image deconvolution approaches, Anal. Chem. 87 (2015) 6125–6132.
[14] V. Hoffmann, G. Ehrlich, Investigations on the lateral distribution of the emission line intensities in the plasma of a Grimm-type glow discharge source, Spectrochim. Acta B At. Spectrosc. 50 (1995) 607–616.
[15] M.R. Winchester, Optically induced analytical error in glow discharge optical emission spectrometry, Appl. Spectrosc. 50 (1996) 245–251.
[16] P. Belenguer, M. Ganciu, P. Guillot, T. Nelis, Pulsed glow discharges for analytical applications, Spectrochim. Acta B At. Spectrosc. 64 (2009) 623–641.
[17] G. Gamez, G. Mohanty, J. Michler, Ultrafast elemental mapping of materials combinatorial libraries and high-throughput screening samples via pulsed glow discharge optical emission spectroscopy, J. Anal. At. Spectrom. 28 (2013) 1016–1023.
[18] V.S. Smentkowski, S.G. Ostrowski, Time of flight secondary ion mass spectrometry: a powerful high throughput screening tool, Rev. Sci. Instrum. 78 (2007) 072215.
[19] M. Voronov, V. Hoffmann, T. Steingrobe, W. Buscher, C. Engelhard, A.P. Storey, S.J. Ray, G.M. Hieftje, Spot patterns and instabilities in a pulsed low-pressure rf glow discharge, Plasma Sources Sci. Technol. 23 (2014) 054009.
[20] M. Kroschk, J. Usala, T. Addesso, G. Gamez, Glow discharge optical emission spectrometry elemental mapping with restrictive anode array masks, J. Anal. At. Spectrom. 31 (2016) 163–170.
[21] M.R. Winchester, M.L. Salit, Design and initial characterization of a glow discharge atomic emission instrument for macro-scale elemental composition mapping of solid surfaces, Spectrochim. Acta B At. Spectrosc. 50 (1995) 1045–1058.
[22] M. Webb, V. Hoffmann, G. Hieftje, Surface elemental mapping using glow discharge - optical emission spectrometry, Spectrochim. Acta B At. Spectrosc. 61 (2006) 1279–1284.
[23] C. Engelhard, S. Ray, W. Buscher, V. Hoffmann, G. Hieftje, Correcting distortion in a monochromatic imaging spectrometer for application to elemental imaging by glow discharge-optical emission spectrometry, J. Anal. At. Spectrom. 25 (2010) 1874–1881.
[24] G. Gamez, S. Ray, F. Andrade, M. Webb, G. Hieftje, Development of a pulsed radio frequency glow discharge for three-dimensional elemental surface imaging. 1. Application to biopolymer analysis, Anal. Chem. 79 (2007) 1317–1326.
[25] M. Voronov, V. Hoffmann, T. Wallendorf, S. Marke, J. Mönch, C. Engelhard, W. Buscher, S. Ray, G. Hieftje, Glow discharge imaging spectroscopy with a novel acousto-optical imaging spectrometer, J. Anal. At. Spectrom. 27 (2012) 419–425.
[26] G. Gamez, D. Frey, J. Michler, Push-broom hyperspectral imaging for elemental mapping with glow discharge optical emission spectrometry, J. Anal. At. Spectrom. 27 (2012) 50–55.
[27] A.P. Storey, S.J. Ray, V. Hoffmann, M. Voronov, C. Engelhard, W. Buscher, G.M. Hieftje, Wavelength scanning with a tilting interference filter for glow-discharge elemental imaging, Appl. Spectrosc. 71 (2017) 1280–1288.
[28] P. Konarski, M. Miśnik, A. Zawada, Two-dimensional elemental mapping using glow discharge mass spectrometry, J. Anal. At. Spectrom. 31 (2016) 2192–2197.

[29] M. Betti, Isotope ratio measurements by secondary ion mass spectrometry (SIMS) and glow discharge mass spectrometry (GDMS), Int. J. Mass Spectrom. 242 (2005) 169–182.
[30] V. Hoffmann, M. Kasik, P.K. Robinson, C. Venzago, Glow discharge mass spectrometry, Anal. Bioanal. Chem. 381 (2005) 173–188.
[31] R. Pereiro, A. Solà-Vázquez, L. Lobo, J. Pisonero, N. Bordel, J.M. Costa, A. Sanz-Medel, Present and future of glow discharge - time of flight mass spectrometry in analytical chemistry, Spectrochim. Acta B At. Spectrosc. 66 (2011) 399–412.
[32] C. Gonzalez de Vega, D. Alberts, V. Chawla, G. Mohanty, I. Utke, J. Michler, R. Pereiro, N. Bordel, G. Gamez, Use of radiofrequency power to enable glow discharge optical emission spectroscopy ultrafast elemental mapping of combinatorial libraries with nonconductive components: nitrogen-based materials, Anal. Bioanal. Chem. 406 (2014) 7533–7538.
[33] S. Litzelman, J. Hertz, W. Jung, H. Tuller, Opportunities and challenges in materials development for thin film solid oxide fuel cells, Fuel Cells 8 (2008) 294–302.
[34] W. Hermes, D. Waldmann, M. Agari, K. Schierle-Arndt, P. Erk, Emerging thin-film photovoltaic technologies, Chem. Ing. Tech. 87 (2015) 376–389.
[35] F. Xiao, C. Hangarter, B. Yoo, Y. Rheem, K. Lee, N. Myung, Recent progress in electrodeposition of thermoelectric thin films and nanostructures, Electrochim. Acta 53 (2008) 8103–8117.
[36] S. Ay, N. Perkgoz, Nanotechnological advances in catalytic thin films for green large-area surfaces, J. Nanomater. (2015) 1–20.
[37] W.F. Maier, K. Stowe, S. Sieg, Combinatorial and high-throughput materials science, Angew. Chem. Int. Ed. 46 (2007) 6016–6067.
[38] Z. Weiss, Calibration methods in glow discharge optical emission spectroscopy: a tutorial review, J. Anal. At. Spectrom. 30 (2015) 1038–1049.
[39] A. Bengtson, T. Nelis, The concept of constant emission yield in GDOES, Anal. Bioanal. Chem. 385 (2006) 568–585.
[40] M. Matsuura, K. Wagatsuma, Two-dimensional observation of emission image of a copper chip excited in a glow discharge plasma, ISIJ Int. 53 (2013) 1923–1926.
[41] G. Gamez, G. Mohanty, J. Michler, Image denoising techniques applied to glow discharge optical emission spectroscopy elemental mapping, J. Anal. At. Spectrosc. 29 (2014) 315–323.
[42] A. Bengtson, Quantitative depth profile analysis by glow discharge, Spectrochim. Acta B At. Spectrosc. 49 (1994) 411–429.
[43] S. Gaiaschi, S. Richard, P. Chapon, O. Acher, Real-time depth measurement in glow discharge optical emission spectrometry: via differential interferometric profiling, J. Anal. At. Spectrom. 32 (2017) 1798–1804.
[44] L. Wilken, V. Hoffmann, K. Wetzig, In situ depth measurements for GD-OES, J. Anal. At. Spectrom. 18 (2003) 1133–1140.
[45] G. Gamez, Compressed sensing in spectroscopy for chemical analysis, J. Anal. At. Spectrom. 31 (2016) 2165–2174.
[46] J.D. Usala, A. Maag, T. Nelis, G. Gamez, Compressed sensing spectral imaging for plasma optical emission spectroscopy, J. Anal. At. Spectrom. 31 (2016) 2198–2206.
[47] M. Glick, G.M. Hieftje, Classification of alloys with an artificial neural network and multivariate calibration of glow-discharge emission spectra, Appl. Spectrosc. 45 (1991) 1706–1716.
[48] R. Martinez, C. Perez, N. Bordel, R. Pereiro, J.L.F. Martin, J.B. Cannata-Andia, A. Sanz-Medel, Exploratory investigations on the potential of radiofrequency glow discharge-optical emission spectrometry for the direct elemental analysis of bone, J. Anal. At. Spectrom. 16 (2001) 250–255.
[49] C. Lazik, K.R. Marcus, Electrical and optical characteristics of a radio frequency glow discharge atomic emission source with dielectric sample atomization, Spectrochim. Acta B At. Spectrosc. 48 (1993) 1673–1689.